Renewable Energy 170 (2021) 1292–1307

Contents lists available at ScienceDirect

Renewable Energy

journal homepage: www.elsevier.com/locate/renene

Determining chaotic characteristics and forecasting tall tower wind speeds in Missouri using empirical dynamical modeling (EDM)

Sarah Balkissoon [a, *], Neil Fox [a], Anthony Lupo [a], Sue Ellen Haupt [b], Y. Charles Li [c], Patrick Market [a], Samuel Walsh [c]

[a] Atmospheric Science Program, School of Natural Resources, University of Missouri, USA
[b] Research Applications Lab, National Center for Atmospheric Research, NCAR, USA
[c] Department of Mathematics, University of Missouri, USA

ARTICLE INFO

Article history:
Received 7 July 2020
Received in revised form
21 January 2021
Accepted 22 January 2021
Available online 29 January 2021

Keywords:
Takens' theorem
Phase portrait
Largest lyapunov exponent
Empirical dynamical modeling
Tall tower wind speeds

ABSTRACT

The chaotic characteristics of the tall tower wind speed data within Missouri was investigated using both quantitative and qualitative methodologies. The phase space diagrams were constructed using the method of time delay. The two parameters needed in the construction of the attractor are the embedding dimension and the time delay. The former was determined using the Cao Algorithm and the latter by Average Mutual Information (AMI). Qualitatively, the phase portraits display chaos for all the wind speed time series for the various stations and height levels. They did not illustrate periodicity nor were they random motions, rather, they depicted a single attractor representative of chaos. Quantitatively the Largest Lyapunov Exponent (LLE) was evaluated. It was determined that for the Columbia station the wind speeds display chaotic characteristics representative of the positive LLEs. However, the increasing level of chaos characteristics did not coincide with the increasing height levels of the tall tower. Thereafter, a simple non-linear prediction algorithm was used to forecast wind speeds using a moving window. The attractor was constructed using the first 56 days and the subsequent 6 h or 36 (10 min) time steps were predicted. The preceding forecast was done when the attractor was reconstructed using the training data of 56 days starting from a 6-h delay from the previous run. The RMSE, MAE and Correlation were investigated for the model with the errors evaluated cumulatively for all of the 1st through 36st predictions. It was determined that the errors increase as the forecasting steps increased for all stations and height levels. The RMSE plateaus at higher wind speeds for increasing height levels with the exception of the station, Neosho, where it plateaued at all height levels at approximately 3.0 ms^{-1}. For Columbia at all height levels, after the 20th time step or 3.33 h, the model's normalized errors exceeds 1 or 100%. However, using a 50% normalized error cap, it was noted that these values occurred for Columbia's height levels after the 1st, 2nd and 3rd time steps respectively. For Blanchard, this value was given by the 2nd time step for both heights whilst for Neosho, at all heights this percentage occurred after at most, 2 time steps. From the Lyapunov exponent, the prediction horizons or the time limits to obtain accurate predictions from the chaotic system were determined to be 6 time steps for all the height levels in the Columbia station using a 95% confidence band. When a range of confidence bands was used, it was shown that for the 90% confidence, this value was decreased to 4 time steps. This model was compared to the benchmark model of persistence where it was determined that the EDM is comparable to persistence and it beats it in the very short-term range of one time step for Columbia and Blanchard. Seasonality and diurnal cycle analyses were also accomplished. Seasonality was investigated by slicing the results every 6 h or extracting every 36th forecast error. It was shown that four of the eight stations' height levels had the season of summer incurring the lowest magnitude of average errors and standard deviations. The diurnal cycle was examined by extracting every four of the 6 time slices done previously. The time of day was analysed by lagging these slices by 6, 12 and 18 h. It was determined that there was no evident trend where a particular time of day the model incurred more errors and had greater standard deviations for all stations and heights.

* Corresponding author.
E-mail address: sarahsharlenebalkissoon@mail.missouri.edu (S. Balkissoon).

https://doi.org/10.1016/j.renene.2021.01.108
0960-1481/

1. Introduction

The prediction of wind speeds can be categorised in either physical, statistical or hybrid methods. The physical methodologies are mathematical models that utilize large amounts of data from numerical weather prediction (NWP). The statistical methods, however, can be classified as either time series, spatial correlations or artificial intelligence procedures whilst hybrid methods combine two or more approaches [8]. Alternative methodologies to conventional predictive methods include the nearest neighbor method of chaos theory, artificial intelligence's neural nets as well as wavelets [19,26].

Chaos theory methodologies are employed in the short-term prediction of forecasting meteorological variables such as wind speed. Short-term wind speed prediction is one of the four temporal ranges of forecast. It is where forecasts are made from one hour to two days ahead and they are used for economic load dispatch planning [8]. This short term prediction is especially important as the adjustments of power generation to a consistently changing load is required and wind is a variable power source. This will ultimately contribute to a steady power supply [15]. These methodologies are sorted after when initial data, needed to build models from first principle is lacking [10]. Thus the time series must be established as chaotic. That is, as defined in Refs. [7,19], it is a simple non-linear deterministic system, which is sensitively dependent on its initial conditions. Such systems display random and complex behaviours. Neural nets use historical data and may use a back propagation technique to adjust its weights. A forecast function is then used to predict future variables using past time series inputs [26]. Finally, wavelets decompose the time series into its various components and then forecast using a weighted sum of these wavelets [26]. These methods have also been combined in complex dynamics forecasting [26].

Natural systems, however, are complex and dynamical, often involving many variables that cannot be measured with sufficient accuracy. If statistical time series models are utilized, these difficulties necessitate the use of non-linear approaches [6] as classical regression analysis cannot fully represent the underlying complex dynamics of especially a chaotic series [26]. A property of non-linear systems is state dependency, which can be defined as the changing relationships among interacting variables with different states associated with the dynamical system [6]. The non-linear statistical methods originates from state space reconstruction which is the lagged co-ordinate embedding of the time series. These methods recover the dynamics of the time series instead of using a set of governing equations. These methodologies are called empirical dynamical modeling [6].

In a study by Ref. [28], many chaos identification methods are used in the determination of a chaotic series. This is done because wind speed has complex characteristics of deterministic and random signals. There are chaos identification methods that are based on phase space reconstruction, which include the phase diagram, correlation dimension and the largest Lyapunov exponent [28]. The phase space method is a qualitative direct chaos identifier method and the correlation dimension and the Lyapunov exponent methodologies are quantitative and direct procedures [29]. If an attractor is non-periodic (the motion of the system never repeats), finite dimensional and generated by deterministic dynamics, then it is a strange or chaotic attractor. Two points on this attractor at a time will be arbitrarily apart from each other at a later time, that is, nearby points in phase space separate at an exponential rate. This is given by the positive largest Lyapunov exponent [2]. In this paper, some of these methods will be employed to identify chaos before a non-linear prediction method, referred to as "Lorenz's method of analogues" [14], is conducted.

The subsequent section, section 2, describes the data utilized in this study. Section 3 outlines the various methodologies used, which are the generation of the wind speed duration curve, the reconstruction of phase space and the determination of the parameters of the embedding dimension and the time delay, the determination of the largest Lyapunov exponent, the forecasting of wind speeds using a non-linear prediction algorithm and the examination of the seasonality and diurnal cycle of the model runs. Section 4 provides the results of the various methods conducted before concluding in section 5.

2. Data

This study uses ten-minute interval daily wind speed time series data recorded in 2009, in ms^{-1}, for Columbia, Blanchard and Neosho, stations in Missouri [11]. Columbia is located in 038° 53.270′ N latitude and 092°15.820′ W longitude and has a site elevation of 255 m. Blanchard is located 040° 33.570′ N latitude and 095° 13.470′ W longitude and has a site elevation of 328 m. Neosho is located 036° 52.730′ N latitude and 094° 25.570′ W longitude with a site elevation of 373 m. Please refer to Fig. 1. The anemometers were placed on various heights and orientations on the towers. For Columbia, Blanchard and Neosho, the anemometer orientations were 120° and 300° for each of the various sites' tall tower heights of 68, 98, 147 m and 61, 97, 137 m and 50, 70, 90 m respectively. Channels 1, 3 and 5 are the wind speed times series of the three consecutive heights at an orientation of 120° and Channels 2, 4 and 6 are wind speed values obtained when anemometers were oriented at 300°. The larger of the wind speed value at each time step for each height level were taken and labelled as Columbia68,Columbia98 and Columbia147, Blanchard61, Blanchard97 and Blanchard137, Neosho50, Neosho70 and Neosho90.

3. Methods

3.1. Wind speed duration curves

Wind speed duration curves (WSDC) provide a simple way to visualize the distribution of wind speeds recorded at the observation sites [20]. They are essentially the graph of the wind speed's cumulative distribution function over the time interval. By convention, the independent variable is along the vertical axis and the horizontal axis is scaled to be a percentage.

More precisely, suppose that $\{x_i\}_{i=1}^n$ is a time series of wind speeds and let $\{z_i\}_{i=1}^n$ be the rearrangement of these values so that they are in ascending order: $z_1 < z_2 < \cdots < z_n$. Here it is assumed for simplicity that the readings are distinct and the observation times are evenly spaced. Then the percentage of time in which the wind speed is greater than or equal to z_i can be approximated by Equation (1).

$$F(z_i) = 100\left(\frac{n+1-i}{n+1}\right) \tag{1}$$

The corresponding WSDC is constructed by plotting the points $(F(z_i), z_i)$ for $i = 1, \ldots, n$.

3.2. Takens' theorem and reconstruction of the phase space

Assume that the weather patterns at the observation sites are governed by a deterministic dynamical system set on a smooth *D*-

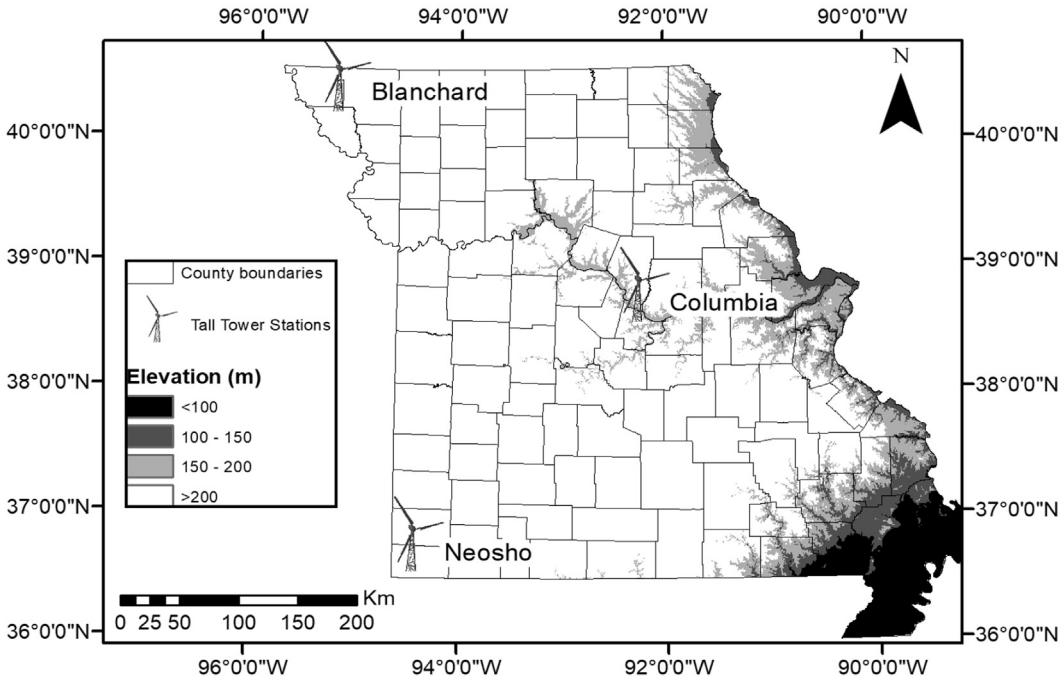

Fig. 1. Study locations within Missouri.

dimensional compact manifold M (the phase space). Let $\varphi_t : M \to M$ denote the corresponding flow map, so that, if the system is initially in state $m \in M$, then $\varphi_t(m)$ is its state after time t.

Weather forecasting is thus equivalent to determining φ_t. However, it is typically difficult to do this directly as the dynamical system is hard to formulate explicitly and it is likely to be nonlinear, high dimensional, and chaotic. Accurately measuring the many variables involved may also prove impractical.

In the seminal paper [27], Takens gives a number of mathematical results addressing this issue. Suppose that $X : M \to \mathbb{R}$ is a scalar-valued observable quantity; for the present study, this will be the wind speed. Under mild assumptions on the regularity of X, Takens shows that it is possible to reconstruct φ_t from the time evolution of the observable $X(\varphi_t)$. Specifically, by [27, Theorem2], for a generic time delay $\tau \geq 0$ and time t, the mapping

$$\Phi_t : m \mapsto (X(\varphi_t),\ X(\varphi_{t+\tau}),\ \ldots,\ X(\varphi_{t+2D\tau}))|_m \tag{2}$$

constitutes a smooth embedding of M into $\mathbb{R}^{2D+1}$. Moreover, in [27, Corollary5] it is established that, for generic $m \in M$, the ω-limit sets of $\Phi_t(m)$ and $\varphi_t(m)$ are diffeomorphic. Stated more plainly: if the full system has an attractor, the topological and differential structure of that attractor can be inferred from the longtime behavior of the time-delay mapping Φ_t.

Suppose now that $\{x_i\}_{i=1}^n$ is a time series representing readings of the observable $X(\varphi_t)$ at equally spaced times $t_1 < t_2 < \cdots < t_n$. For candidate embedding dimension d and time delay τ, in analogy to (2), one forms the Takens reconstruction vector

$$y_i = (x_i,\ x_{i+\tau},\ \ldots,\ x_{i+(d-1)\tau}) \tag{3}$$

with index $i = 1, 2, \ldots, N$ and $N = N(\tau, d) = n - (d-1)\tau$. Note that in what follows the dependence of N on τ and d is often suppressed for the sake of simplifying the notation. Provided that $d \geq 2D + 1$, Takens' embedding theory can then be used to predict the dynamics of the original system from the delayed time series $\{y_i\}_{i=1}^N$.

This leads to the statistical problem of choosing the parameters τ and d, which has been the subject of considerable research. Even though Takens' theorem holds for a generic time delay, it is well known that some care is required in selecting τ when working with experimental data. If the time delay window is too narrow, then the attractor will be projected into a dimension that is too small. Were this to occur, then x_{i+1} will not contain substantially new information relative to x_i, making predictions based on the time series unreliable [25]. Conversely, if the window is too large, the components of y_i become noisy [4,16] making accurate forecasting difficult [25]. The next two subsections outline the approach to these questions taken in this work.

3.3. Estimate of the embedding dimension via Cao's algorithm

Common technique for selecting the embedding dimension include the method of False Nearest Neighbours (FNN) [4,17] and Cao's Algorithm [5]. FNN, which is used in Ref. [16], for example, involves tracking the number of points in the reconstructed time series $\{y_i\}$ that appear to be nearby only because the embedding space is too small. The embedding dimension is taken to be the minimal d so that the number of these "false neighbours" is zero.

In this paper, Cao's Algorithm was used to determine the embedding dimension. Compared to FNN, it has the advantage of being less sensitive to the number of points in the time series, and it does not introduce any subjective parameters [5]. Moreover, it can differentiate between deterministic (no uncertainty with respect to time) and stochastic (random signals that cannot be written in mathematical equation) time series [5].

The method can be described as follows. Given a time series $\{x_i\}_{i=1}^n$, let $\{y_i^d\}_{i=1}^{N(\tau,d)}$ and $\{y_i^{d+1}\}_{i=1}^{N(\tau,d+1)}$ be the reconstructed time series given by equation (3) for the candidate embedding dimensions d and $d+1$, respectively. For each $1 \leq i \leq N - d\tau$, let $y_{n(i,d)}^d$ be the nearest neighbor to y_i^d (that is distinct from y_i^d) with distance measured in the max norm on $\mathbb{R}^d$, and define $n(i, d+1)$

accordingly. As in Ref. [5], we set

$$a(i,d) = \frac{\left\| y_i^{d+1} - y_{n(i,d)}^{d+1} \right\|}{\left\| y_i^{d} - y_{n(i,d)}^{d} \right\|} \tag{4}$$

where $\|\cdot\|$ is the max norm, and consider the average of this quantity over i:

$$E(d) = \frac{1}{N - d\tau} \sum_{i=1}^{N-d\tau} a(i,d). \tag{5}$$

Two points that are close in d-dimensional reconstructed phase space and also close in $(d+1)$-dimensional reconstructed phase space are called true neighbours [5]. This is measured by means of the function

$$E1(d) = \frac{E(d+1)}{E(d)}. \tag{6}$$

Observe that $E1(d)$ will be constant when $d \geq 2D+1$, and hence it can be used to identify the minimum embedding dimension [5].

A second consideration that is important for applications is whether the data is stochastic or deterministic. For this, Cao introduces the function

$$E2(d) = \frac{E^*(d+1)}{E^*(d)} \tag{7}$$

where

$$E^*(d) = \frac{1}{N - d\tau} \sum_{i=1}^{N-d\tau} \left| x_{i+d\tau} - x_{n(i,d)+d\tau} \right|.$$

If the data are deterministic then $E2(d)$ is dependent on d and so one will observe that $E2(d) \neq 1$ for some choice of d. On the other hand, if the data is random, then it must hold that $E2(d) = 1$ for all d. Computing both $E1(d)$ and $E2(d)$ allows one to both find a reasonable embedding dimension and also offers evidence that the underlying process is indeed deterministic [5].

3.4. Time delay estimation via Average Mutual Information

An appropriate time delay can be determined through the use of an Autocorrelation Function (ACF) or considering the Auto Mutual Information (AMI) [4]. This paper uses the latter technique, which was first introduced by Fraser and Swinney [12]. This method was used because of its ability to measure the general rather than linear dependence of two variables [12]. It is also a common methodology used in the construction of the phase space of the attractor [30].

Let $\mathscr{A}$ and $\mathscr{B}$ be discrete sets. For a random vector (A,B) with state space $\mathscr{A} \times \mathscr{B}$ and discrete joint probability distribution P_{AB}, the mutual information of the random variables A and B is defined by

$$I_{AB} = \sum_{a \in \mathscr{A}} \sum_{b \in \mathscr{B}} P_{AB}(a,b) \log_2 \left(\frac{P_{AB}(a,b)}{P_A(a) P_B(b)} \right), \tag{8}$$

where P_A and P_B are the marginal probabilities for A and B, respectively. Intuitively, I_{AB} measures on average how accurately one can determine B given knowledge of A (or vice versa). The idea of AMI is to treat $X(\varphi_t)$ and $X(\varphi_{t+\tau})$ as random variables, then adjust τ so as to maximize their mutual information.

With that in mind, suppose $\{x_i\}_{i=1}^n$ is a (portion of a) time series obtained from experimental data. For a candidate time delay τ, we form the shifted series $\{x_{i+\tau}\}_{i=1}^n$ and introduce the sets $\mathscr{A} = \{x_i : i = 1, \ldots, n\}$ and $\mathscr{B} = \{x_{i+\tau} : i = 1, \ldots, n\}$. Let (A,B) be the random vector taking values on $\mathscr{A} \times \mathscr{B}$ whose probability distribution P_{AB} is generated by a histogram of $\{(x_i, x_{i+\tau})\}_{i=1}^n$ with an appropriate bin size. The mutual information of the components A and B as a function of τ is thus

$$I(\tau) = \sum_{i,j=1}^{n} P_{AB}(x_i, x_{j+\tau}) \log_2 \left(\frac{P_{AB}(x_i, x_{j+\tau})}{P_A(x_i) P_B(x_{j+\tau})} \right). \tag{9}$$

We choose the value of τ to be the either the first local minimum of I or when the AMI is monotonically decreasing to the ratio of $\frac{I(\tau)}{I(0)} = 0.2$ or $\frac{1}{e}$ [17].

3.5. Largest Lyapunov Exponent (LLE)

The characterizing feature of chaotic systems is that future states are effectively unpredictable despite the underlying dynamics being deterministic. This phenomenon stems from the flow map φ_t exhibiting sensitive dependence on initial conditions (SDOIC) [14]. Lyapunov exponents provide one way to quantify this SDOIC [22] and thereby gauge how chaotic a system is [14]. Trajectories that are initially close but lie on a chaotic attractor will diverge from one another exponentially fast; the Lyapnuov exponent λ gives the average rate of this divergence [13,22]. Note that it is essential here to take an average since the rate will potentially be different in different directions [14].

As Lyapunov exponents are insensitive to the choice of metric, they can be computed through consideration of the Takens' flow. For a point $m \in M$ and time t, we define the Lyapunov exponents to be the eigenvalues of the linearized flow map there; the eigenvalue with largest real part is called the largest Lyapunov exponent (LLE) and denoted λ. Note that the dynamics of the attractor — should one exist — is dissipative and as such the sum of the Lyapunov exponents is negative there. Conversely, in the applied literature, a positive Lyapunov exponent is often taken as sufficient evidence that the system is chaotic [3,7,22]. By contrast, if $\lambda < 0$, then there exists (asymptotically) stable fixed points to which one will find trajectories converging exponentially. If one has trajectories that approach or separate from each other slower than an exponential rate, there must exists a limit cycle that is marginally stable; in this case, the LLE is equal to zero [14]. Finally, for random noise, the LLE can be thought of as infinite [14].

Let $\Delta(t)$ be the distance between two points in phase space for the embedded map at time t. Then

$$S(t) = \ln \frac{\Delta(t)}{\Delta(0)} \tag{10}$$

provides an approximate upper bound on λt. To determine $S(t)$ from the time series, we construct a Takens vector, say, y_{N_0} and construct a neighbourhood about this vector of ε distance, $B_\varepsilon(y_{N_0})$. For each of the nearby Takens vectors, y_i, $i = 1, \ldots, N$, the average error between a forward time step, δT, of both a nearby Taken vector $(x_{i+\delta T})$ and the fixed Taken vector, y_{N_0} $(x_{N_0+\delta T})$ is determined. The logarithm of all the average distances are taken to give a measure of the exponential rate of expansion. The average of all N_0 values are used to smooth out any noise [14]. From Kantz and Schreiber [14], $S(t)$ is given by

$$S(t) = \frac{1}{N} \sum_{N_0=1}^{N} \ln \left(\frac{1}{\left| B_\varepsilon(y_{N_0}) \right|} \sum_{\substack{i=1,\ldots,N: \\ y_i \in B_\varepsilon(y_{N_0})}} \left| x_{N_0+\delta T} - x_{i+\delta T} \right| \right). \tag{11}$$

The largest Lyapunov exponent is estimated by the slope of the linear region of the curve of $S(t)$ against t [13]. After the linear region, the curve saturates for large t values since the system is bounded in phase space [22].

This method has been proven by Ref. [22] to work well with smaller time series as well as time series with white noise superimposed with noise-free data. This is especially important, as shown in Ref. [9], where the length of a series and quality are factors in the accuracy of the extraction of dynamical information.

If the system is chaotic and $\lambda > 0$, then the series can be predicted with a prediction horizon given by

$$t^* = \frac{1}{\lambda} \ln 1.96 \tag{12}$$

where t^* is the maximum amount of samples with sampling time that can be predicted with uncertainty; see, for example, [7]. The uncertainty used is 1.96ε which represents a 95% confidence band. The confidence bands of 90% and 99% were also evaluated in this study. The forecasting error exponentially increases with the forecasting time at a rate given by the LLE [7]. Thus we see that even though chaos places a limit on long-term prediction, it affords the ability of short term prediction [10].

3.6. Forecasting using simple non-linear prediction algorithm

The future state of the system is a function of the present state at some time say, t. That is, there exists a deterministic forecasting function [14]. Since there is no certainty of our present state, inaccuracies grow exponentially over time in chaotic systems. However, the uncertainties increased over a finite rate, even for chaotic systems, and as such, short term forecasts can be made [14].

Consider a scalar time series given by $\{x_i\}_{i=1}^{n}$. Fixing a time delay τ and embedding dimension d, we form the reconstruction vectors $\{y_i\}_{i=1}^{N}$ according to (3). To predict some time δt ahead, we consider $B_\varepsilon(y_N)$, the d-dimension ball centered at y_N with radius ε. In this analysis, ε was chosen to be half the smallest possible reading of the anemometer, 0.05. For all the points y_i lying in this ball, we find their corresponding individual prediction values δt ahead, then average the result. The prediction is given by

$$x_{N+\delta t} = \frac{1}{|B_\varepsilon(y_N)|} \sum_{\substack{i=1,\ldots,N; \\ y_i \in B_\varepsilon(y_N)}} x_{i+\delta t}, \tag{13}$$

which represents the average of these values [14].

Thus we see that the feature of the attractor being a compact object in phase space, and thus, having neighbours is utilized in the prediction of the time evolution of new points on or nearby the attractor [16].

3.7. Errors

In order to test the accuracy of the forecast, the root mean square error (RMSE) and mean absolute error (MAE) were computed. These are given by the following equations.

$$\mathrm{RMSE} = \sqrt{\langle (p_n - x_n)^2 \rangle}, \quad \mathrm{MAE} = \langle |p_n - x_n| \rangle,$$

where p_n is the predicted observation whilst x_n is the actual observation at the time step n.

The normalized errors were also computed via

$$E = \frac{\sqrt{\langle (p_n - x_n)^2 \rangle}}{\sqrt{\langle (x_n - \bar{x})^2 \rangle}} = \frac{\mathrm{RMSE}}{\mathrm{SD}}. \tag{14}$$

Here $\bar{x} = \frac{1}{n}\sum_{i=1}^{n} x_i$ is the mean of the time series. If $E = 0$ or 0%, then the prediction is perfect. At the other extreme, if $E = 1$ or 100%, then the prediction is no better than the mean [10].

3.8. Analysis of seasonality and the diurnal cycle

The seasonality effects on the forecast were investigated. For Columbia, Blanchard and Neosho sites the results including the forecast error, found by subtracting the predicted value from the actual value, were sliced for every 36th value. This represents every 6th hour of data. Mathematically, this was given by $36n + 6$. For Columbia the sequence $n = 0, 1, 2, 3, \ldots, 1237$ accounted for its time series of length 44568. Thus, we had a slice of wind speed values, say x_i whose subscript values i range from $i = 6, 42, 78, \ldots, 44538$. For Blanchard, $n = 0, 1, 2, 3, \ldots, 738$ which ran through the series with 26604 data points. Also Neosho has values $n = 0, 1, 2, 3, \ldots, 991$ and a series length of 35712.

The diurnal effects of the forecast were also examined in this study. This was done by further slicing of every 4th 6 h time slice given above. This is represented as $4m + 1$. It can also be established by slicing of the original data set, $144m + 6$ where $m = 0, 1, 2, 3, \ldots, 309$ for Columbia, $m = 0, 1, 2, 3, \ldots, 184$ for Blanchard and $m = 0, 1, 2, 3, \ldots, 247$ for Neosho. Thus, for Columbia, the indices considered from the wind speed error were 6, 150, 294, 438, …, 44502 (the last value can be given by $144 \times 309 + 6$). For Blanchard and Neosho, the subscript sequence is the same with the exception of the upper limit being 26502 for Blanchard and 35574 for Neosho.

This $144m + 6$ slice of the data was then lagged 6, 12 and 18 h using the following algorithms $36 + [144m + 6], 72 + [144m + 6]$ and $108[144m + 6]$. This was done to investigate the relationship between the time of day and the errors in the forecast for all height levels and stations within the forecast run of 2009. For Columbia station, for the 6 h (36 10-min), 12 h (72 10-min) and 18 h (108 10-min) shifts, the sequences are given by 42, 186, 330, 474, …,44538 and 78, 222, 366, 510, …, 44430 and 114, 258, 402, 546, …, 44466 respectively. The same sequences were done for Blanchard and Neosho, however their upper limits were 26538, 26574, 26466 and 35610, 35646, 35682 for 6, 12 and 18 h shifts correspondingly.

4. Results

4.1. Wind speed duration curve (WSDC)

The WSDC is a graphical analysis tool for the persistence of energy production for a particular station [20]. Figs. 2–4 depict the WSDC for the various stations, Columbia, Blanchard and Neosho and their individual tower heights for the year 2009. From the graphs we observe that there is more of a wind speed variability among the height levels for Columbia when compared to Neosho. This is expected as Columbia station's tower spans greater height levels than Neosho. It is also observed that Blanchard97 experiences a constant low value of wind speed well below 5 ms^{-1} for approximately 50% of the time. For the various stations and tall towers, if the WSDC is flatter, then the wind regime is more regular, if not it is more irregular. From the results obtained, it can be noted that the wind regime is more irregular as the heights are increased for both Columbia and Blanchard with the exception of Blanchard97. From Table 1, the percentage of time the wind speeds are greater than or equal to 4 ms^{-1}, which is typically less than the

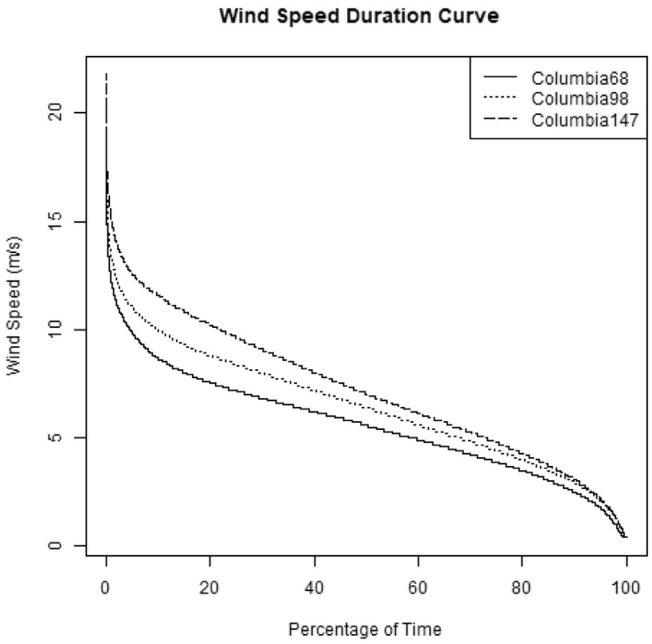

Fig. 2. WSDC for Columbia station.

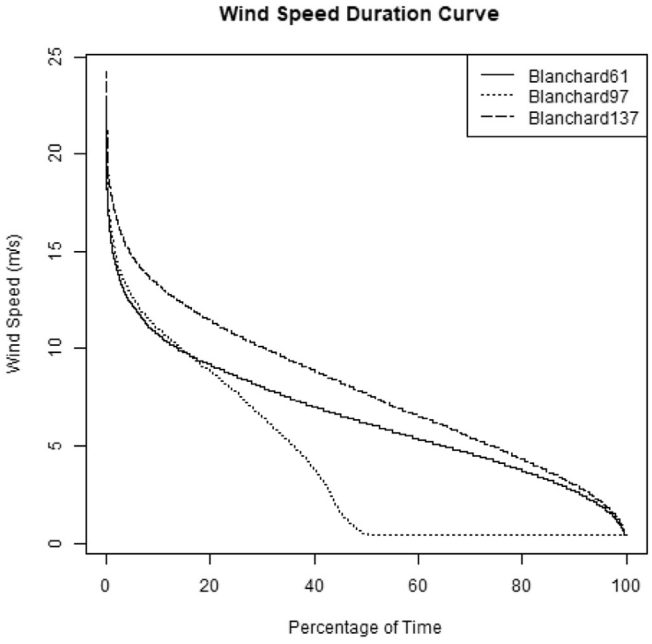

Fig. 3. WSDC for Blanchard station.

turbine cut-in wind speed [23], were higher than 70% excluding Blanchard97. This indicates relatively significant energy persistence for the stations studied. The energy persistence increased with height for stations Columbia and Blanchard neglecting the intermediate height level of Blanchard, Blanchard97. This was not the case for Neosho.

4.2. Reconstruction of phase space

The two parameters, τ and d, for the various months and height levels for the year of 2009 at Columbia are given by Table 2.

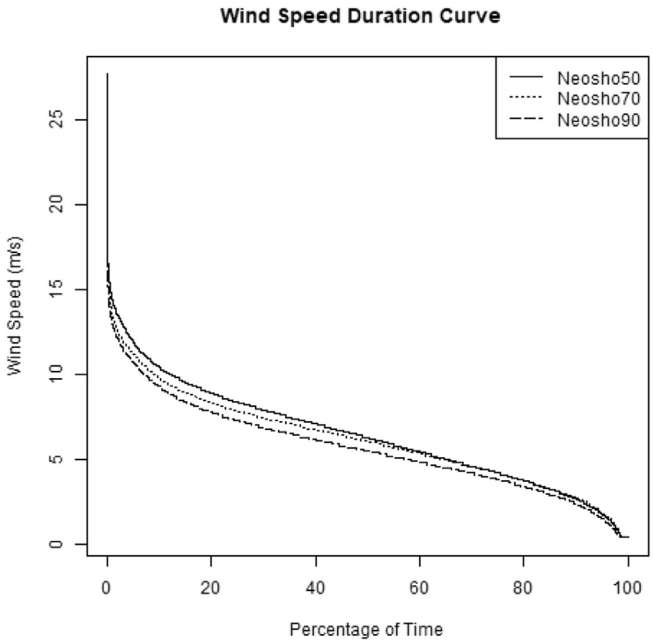

Fig. 4. WSDC for Neosho station.

However, for illustrative purposes we show the results of August consistently throughout the paper. This, as well as the other results, depicts both qualitatively and quantitatively, the chaotic nature of the series. From Figs. 5–7, we see that at Columbia for the month of August at height levels 68, 98 and 147 m, the first local minima (τ) were observed at 5, 5 and 6 respectively. Similarly, for the corresponding embedding dimensions in August, given by Figs. 8–10 are 9, 9 and 8. It is observed that $E1(d)$ attains saturation at these values. Also, $E2(d)$ is related to $E1(d)$ and there exist some values of d for which $E2(d) \neq 1$. This implies that the data are deterministic rather than random. From the results obtained we note that there are τ and d values that repeat for this station. Such findings are indicative of required dimensional construction of phase space to capture the underlying dynamics of the system [30]. Given that the values for d is for most cases 9, it indicates that the ease of predictability will be similar for this station for all months as dynamics of lower dimensions are easier to predict [19].

The phase portraits or diagrams as seen in Figs. 11–13 depict the non-linear variation of the state of the system with time for Columbia at three different heights. It gives the attractor's spatial structure [28]. The axes represent the first three time delayed coordinates used in the construction of the attractor which can be shown diagrammatically. The number of time delayed, τ, coordinates is determined by the embedding dimension, d. Since the trajectories from the system phase space did not show periodicity nor were they random motion but rather illustrated a single attractor, the time series displays chaotic characteristics. These are deterministically chaotic systems. This is shown in also in a study by Zend et al. [29] in which the phase diagram of near surface winds were not closed curves indicative of aperiodic trajectories. In another study done by Yu et al. [28], the trajectories of the attractor were not as well-defined as that of Lorenz's because the interference of noise signals from the environment. For all of the months in 2009 and height levels of the tall tower in Columbia, we observed the chaotic characteristics of the wind speed from the phase portraits.

Table 1
Wind Speed Values greater than or equal to 4 ms^{-1} from WSDC.

$y(m/s)$	Station	$x(\%)$
4	Columbia68	73.4
	Columbia98	79.9
	Columbia147	82.7
4	Blanchard61	77.1
	Blanchard97	39.5
	Blanchard137	82.5
4	Neosho50	77.2
	Neosho70	77.1
	Neosho90	72.5

Table 2
Values of the Parameters, time delays and embedding dimensions for Columbia station.

Month	τ	d	Month	τ	d	Month	τ	d
Jan C68	10	8	Feb C68	6	8	Mar C68	5	9
Jan C98	4	11	Feb C98	6	9	Mar C98	5	9
Jan C147	1	9	Feb C147	6	8	Mar C147	6	9
Apr C68	5	9	May C68	5	9	June C68	4	9
Apr C98	5	9	May C98	5	9	June C98	5	9
Apr C147	5	9	May C147	6	9	June C147	5	8
July C68	4	9	Aug C68	5	9	Sept C68	7	8
July C98	4	9	Aug C98	5	9	Sept C98	7	8
July C147	5	9	Aug C147	6	8	Sept C147	8	7
Oct C68	5	9	Nov C68	5	9	Dec C68	6	9
Oct C98	6	9	Nov C98	5	9	Dec C98	6	8
Oct C147	7	9	Nov C147	6	8	Dec C147	7	8

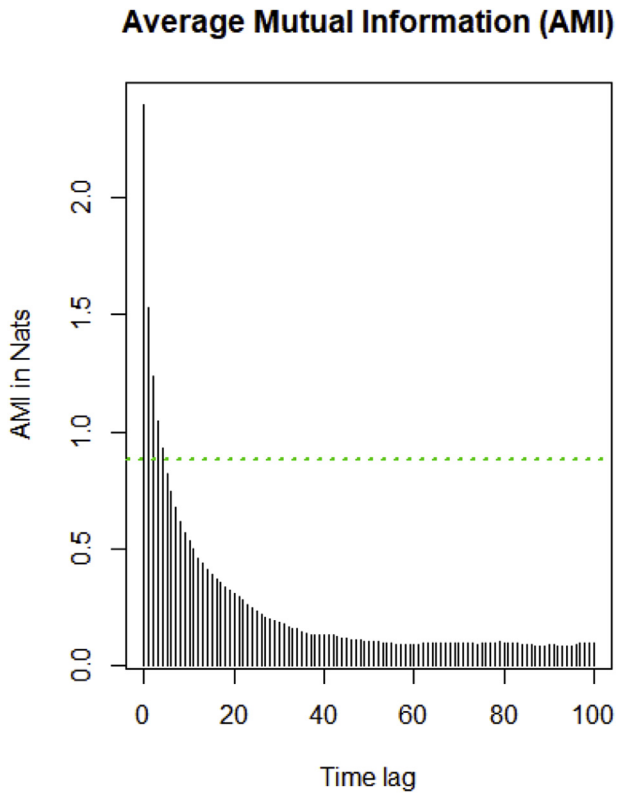

Fig. 6. Time delay given by the method of AMI, Mutual Information against Time Lag for Aug Columbia98.

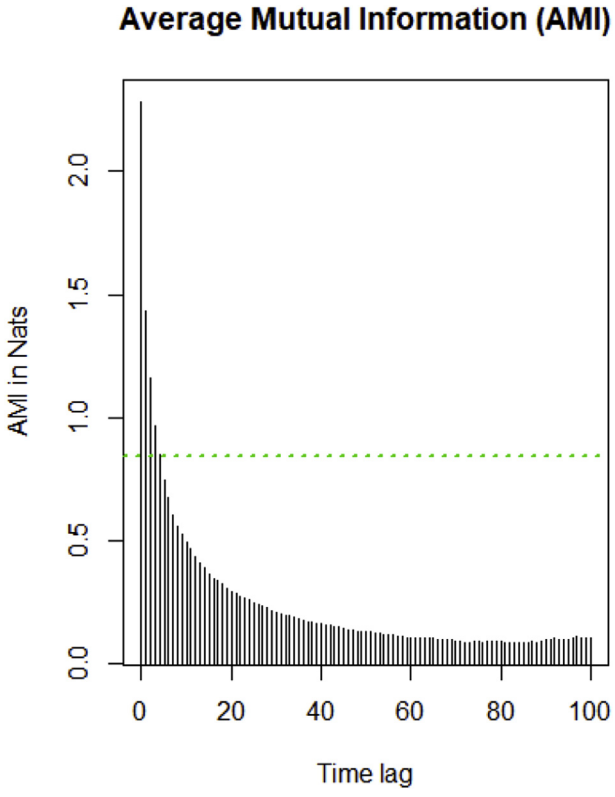

Fig. 5. Time delay given by the method of AMI, Mutual Information against Time Lag for Aug Columbia68.

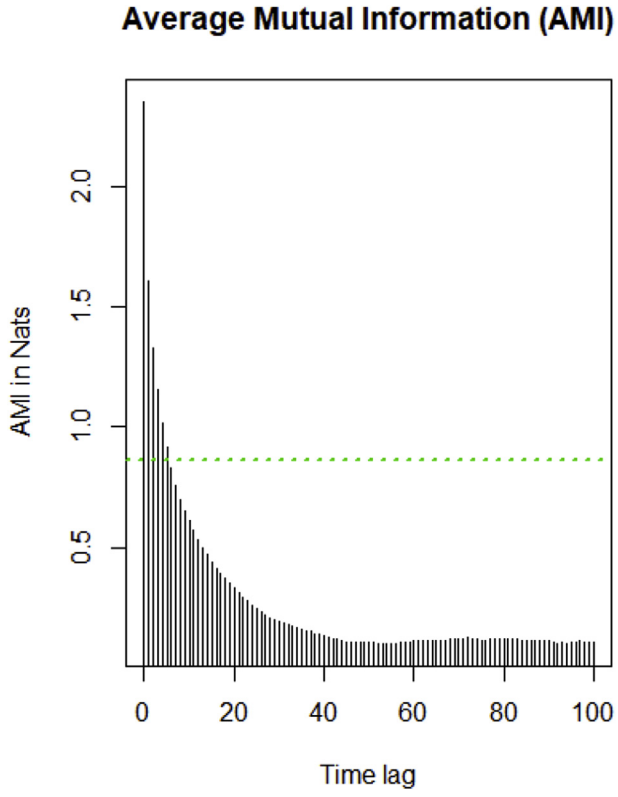

Fig. 7. Time delay given by the method of AMI, Mutual Information against Time Lag for Aug Columbia147.

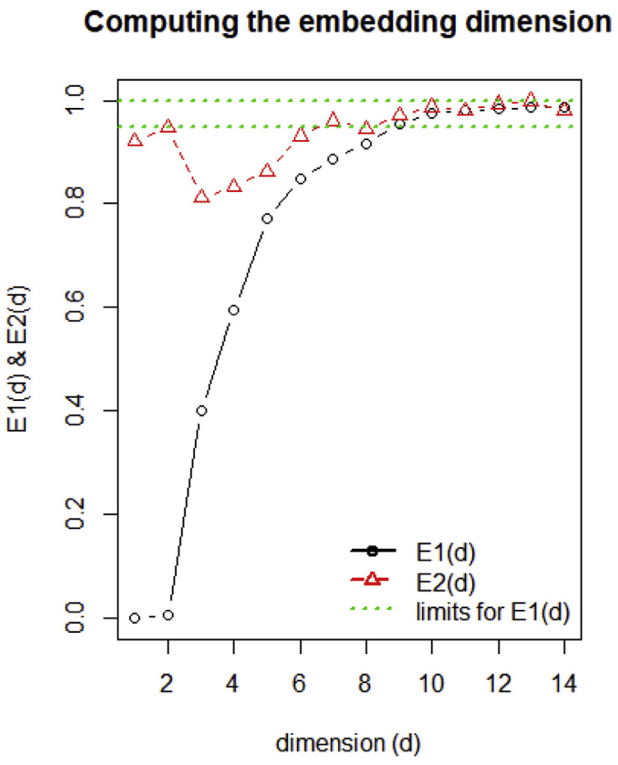

Fig. 8. Embedding dimension given by Cao's Algorithm, $E1(d)$ and $E2(d)$ against d for Aug Columbia68.

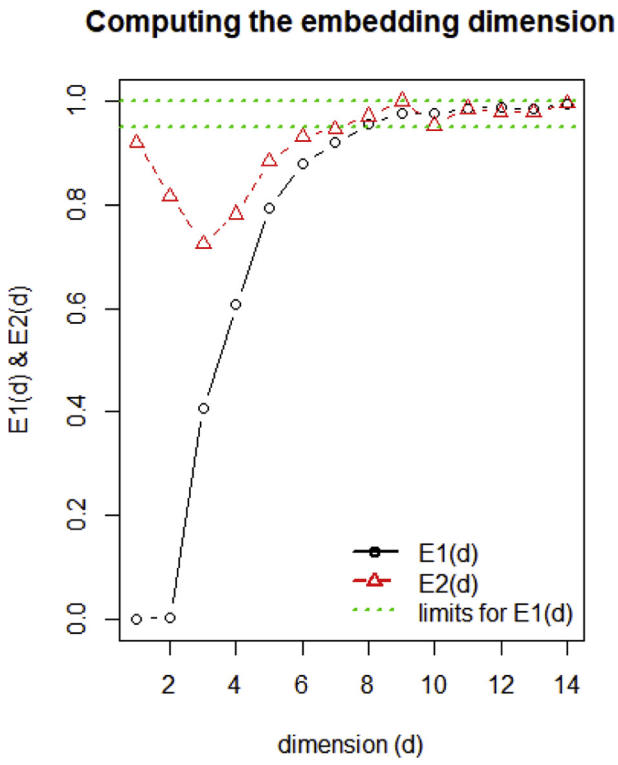

Fig. 10. Embedding dimension given by Cao's Algorithm, $E1(d)$ and $E2(d)$ against d for Aug Columbia147.

4.3. Largest Lyapunov Exponent (LLE)

The wind speed at all heights of the tall tower display chaotic characteristics as the LLE were positive [14]. This implies that the trajectories diverge exponentially fast and there is an increase in the average exponent of the trajectory divergence characteristic of a non-periodic system as also seen in the phase diagrams of this study. From the graphs in Figs. 14–16, it can be noted that even though it is not prominent, there is a linear region before the curve saturates regardless of the embedding dimensions. It is also seen in a study done by Yu et al. [28] that wind speeds display positive chaotic characteristics. In this study however, the increasing level of chaos characteristics did not coincide with the increasing height levels of the tall tower. This is noted quantitatively from Table 3.

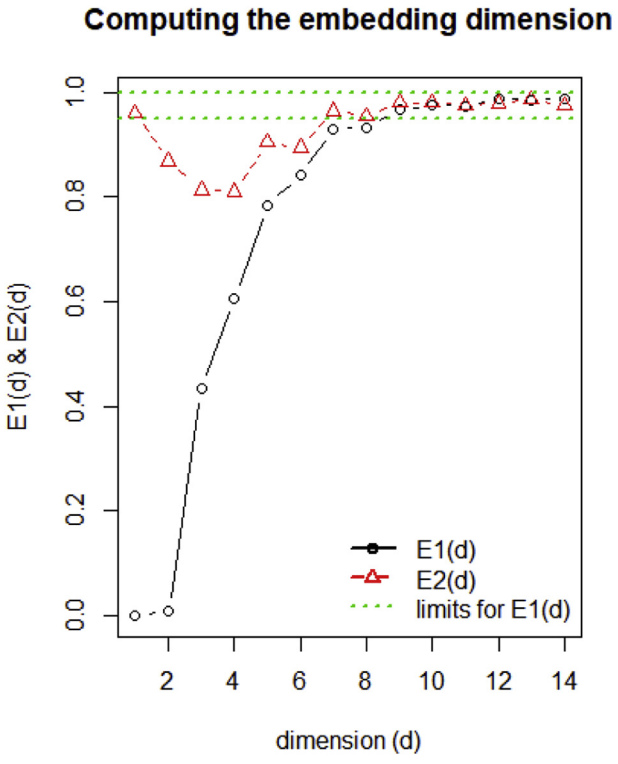

Fig. 9. Embedding dimension given by Cao's Algorithm, $E1(d)$ and $E2(d)$ against d for Aug Columbia98.

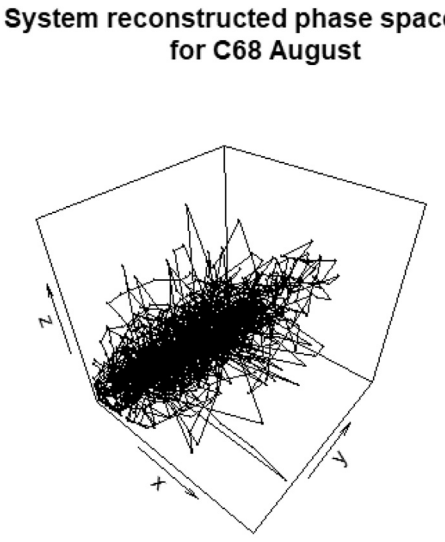

Fig. 11. Phase space reconstruction for Aug Columbia68 showing the first three time delayed co-ordinates.

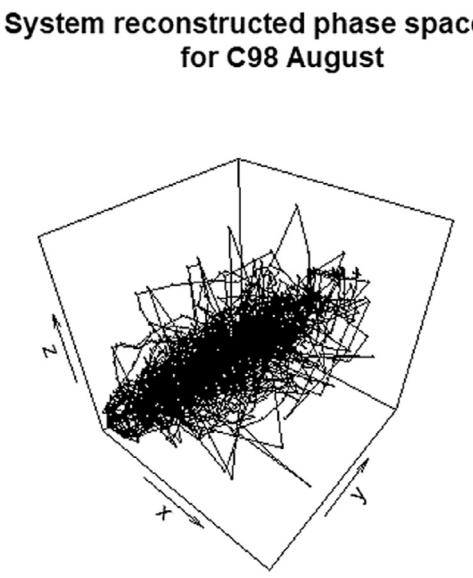

Fig. 12. Phase space reconstruction for Aug Columbia98 showing the first three time delayed co-ordinates.

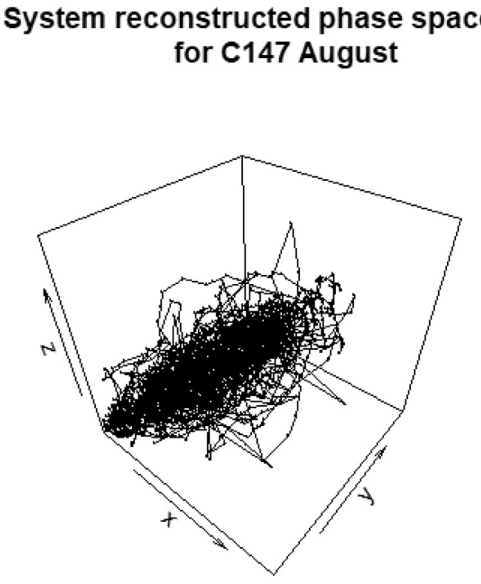

Fig. 13. Phase space reconstruction for Aug Columbia147 showing the first three time delayed co-ordinates.

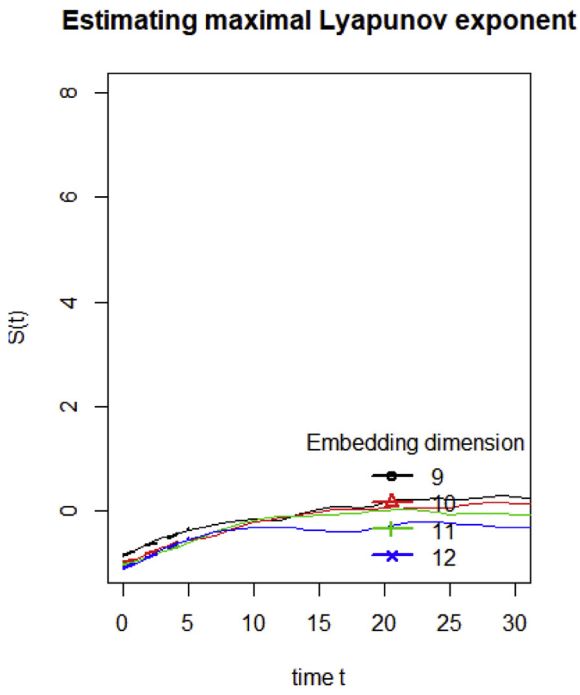

Fig. 14. Lyapunov Exponents for Aug Columbia68, $S(t)$ against t.

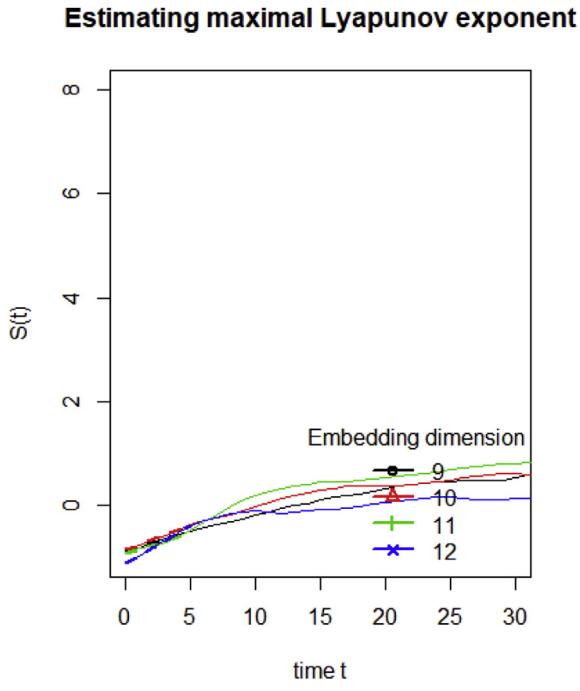

Fig. 15. Lyapunov Exponents for Aug Columbia98, $S(t)$ against t.

The average LLE of the various tall tower heights for the 2009 were 0.1133, 0.11305 and 0.11259 for Columbia68, Columbia98 and Columbia147 respectively. From equation (12), we obtain the prediction horizon to be approximately 6 times steps or one hour for all height levels. However, changing the confidence band to 90% and 99%, decreased and increased the prediction horizon to approximately 4 and 8 time steps respectively. Thus, we note an incremental increase in the prediction horizon by 2 time steps when the confidence bands increased from 90 to 95 and to 99%. We expect this increase as increasing the confidence causes an increase in the margin of error thus resulting in a larger interval. If we consider the minimum of all the LLE of each of the increasing height levels, we get the corresponding values of 0.07613, 0.06329 and 0.06452. The prediction horizon, using the 95% confidence band, is increased to approximately 9, 11 and 10 time steps or 1.5, 1.8 and 1.6 h respectively. Similarly using these minimum LLE, it was determined that for the two largest height levels of this station, for a confidence band of 99%, the prediction horizon increased to an estimated 2.5 h. Whilst using the lowest confidence band of 90%, the said value was decreased to approximately 1.3 h. For the lowest height level, confidence bands of 90 and 99% implied roughly 1.2 and 2 h for the prediction horizon respectively.

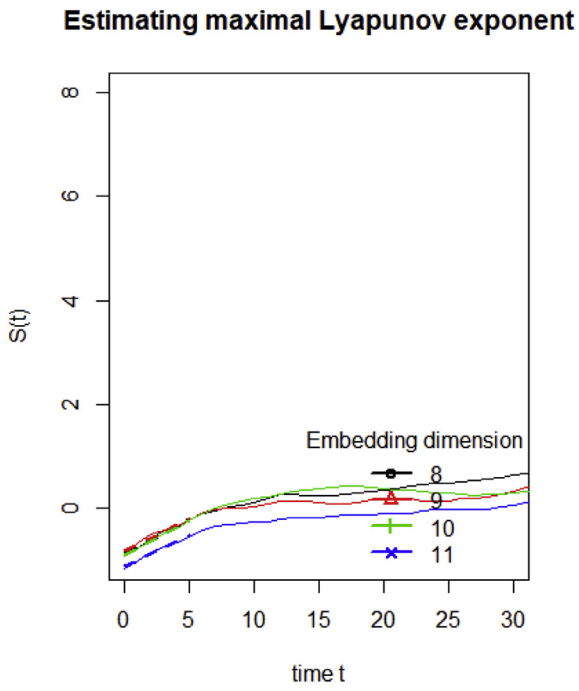

Fig. 16. Lyapunov Exponents for Aug Columbia147, $S(t)$ against t.

Table 3
Values of the Parameter, Lyapunov Exponent, for Columbia station.

Month	LLE	Month	LLE	Month	LLE
Jan C68	0.21850120	Feb C68	0.11124360	Mar C68	0.12129040
Jan C98	0.23026360	Feb C98	0.06329283	Mar C98	0.10560540
Jan C147	0.28907590	Feb C147	0.09144223	Mar C147	0.08357779
Apr C68	0.11611450	May C68	0.10797860	June C68	0.09807250
Apr C98	0.09545526	May C98	0.07794641	June C98	0.09980393
Apr C147	0.09965277	May C147	0.06451961	June C147	0.11250640
July C68	0.14193490	Aug C68	0.09708272	Sept C68	0.08012870
July C98	0.13593250	Aug C98	0.09956517	Sept C98	0.13722600
July C147	0.06720401	Aug C147	0.12664330	Sept C147	0.10288420
Oct C68	0.11155650	Nov C68	0.07613265	Dec C68	0.07952253
Oct C98	0.10451390	Nov C98	0.07777989	Dec C98	0.12927020
Oct C147	0.10715060	Nov C147	0.11311340	Dec C147	0.09325161

4.4. Forecasting using non-linear algorithm

For this forecasting analysis, all the height levels of each station were employed. The attractor was constructed using the first 56 days of the year having determined the embedding dimension and the time delay using that data as the training of the model. Using the forecasting algorithm described in section 3.4, the next 6 h or 36 time steps (in 10 min intervals) were predicted. The preceding forecast was done for the next consecutive 6 h but it was done using a moving window in which the attractor was reconstructed for this run. The training data were assigned to be 56 days starting from a six hour delay of the previous run. This process was iterated until the entire series in this moving window is accounted for. The forecasted data for each run and the actual data were compared and its RMSE, MAE and Correlations were calculated. These errors were determined cumulatively for all of the first predictions or time step through the last prediction or 36th time step.

From the results given in Figs. 17–19 for all of the height levels in Columbia, it is evident that both the RMSE and the MAE increases as the forecasting time step is increased as expected. It should be noted that the correlation between the actual and the predicted wind speed values is greatest (almost 1) at the first time step and it decreases to under 0.5 for the last time step. It is observed that the RMSE plateaus to approximately 2.5 ms^{-1}, 3.0 ms^{-1} and 3.5 ms^{-1} for Columbia68, Columbia98 and Columbia147 respectively. The errors are expected to increase as the height level increases because the wind speeds are increasing with height.

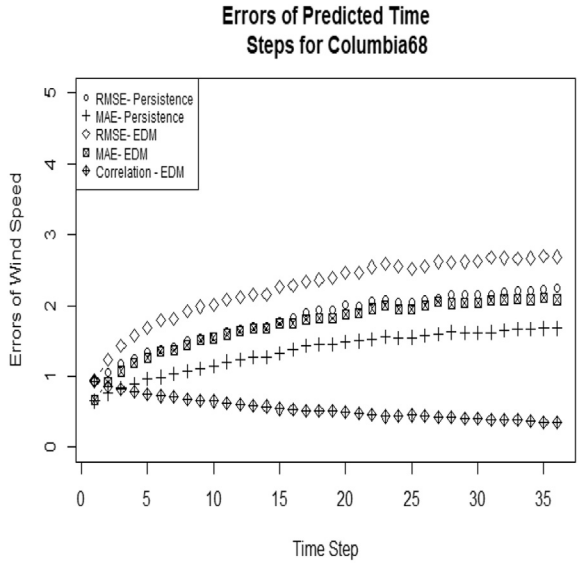

Fig. 17. Errors and correlations for Columbia68, RMSE (ms^{-1}), MAE (ms^{-1}) and correlations against time step for EDM and persistence.

Similar analyses were done in Figs. 20 and 21. However, no results are provided for Blanchard97 because of its inoperability for approximately 50% of the time. The max RMSE for Blanchard61 and Blanchard137 were greater than Columbia; their values for the 36th forecasts were approximately 3.5 and 4.5 ms^{-1}. For the Neosho tall tower, as depicted in Fig. 21, the RMSEs for the last prediction step were 3.17, 2.96 and 2.87 ms^{-1} for Neosho50, Neosho70 and Neosho90 respectively. This is approximately 3.0 ms^{-1} for all heights. This as well as the similar numerical trends from the other time steps, indicate that of all the stations, there is least variability between the actual and predicted values for this station. This coincides with Fig. 4, where Neosho had the least wind speed variability among all the height levels.

Figs. 22–24 show the normalized errors for the various stations. All of the stations and at all heights follow the same increasing trend, which begins to plateau. From the results of Columbia, for all of the heights, after the 20th time step or after 3.33 h of forecasting, the model normalized errors exceed 1 or 100%. As such the forecast is no better than the mean of the data after this run. However using a range of normalized errors, we note that for normalized errors exceeding 50 and 75% occurred after the 1st, 2nd, 3rd and the 7th, 7th, 9th time steps for Columbia68, Columbia98 and Columbia147 respectively. From the Lyapunov analysis, the prediction horizon was determined to be 4, 6 and 8 time steps for the various confidence bands, which all gave normalized errors of less than 65, 75 and 80% correspondingly. Similarly, for Blanchard61 and Blanchard137, the normalized error was below this 100% normalized error threshold at the 22nd and 19th time step respectively. The 8th and 2nd time steps corresponded to normalized errors of under 75 and 50% respectively. Also for Neosho, this model is not better than the average projection after the 23rd, 24th and 27th 10-min forecast for Neosho50, Neosho70 and Neosho90 correspondingly. However the normalized errors of under 50 and 75%, for these

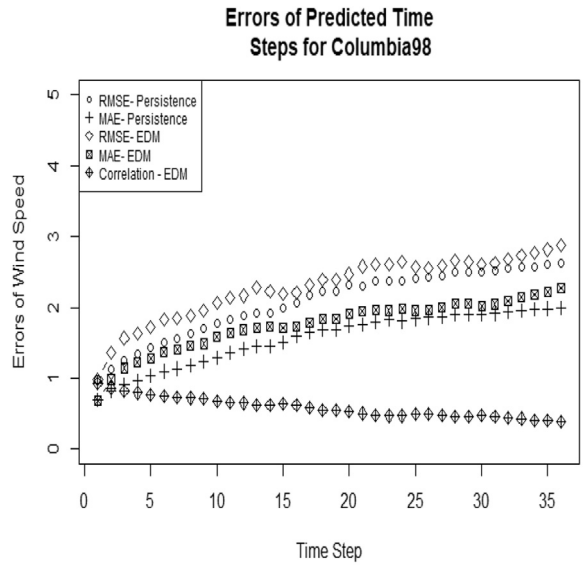

Fig. 18. Errors and correlations for Columbia98, RMSE (ms^{-1}), MAE (ms^{-1}) and correlations against time step for EDM and persistence.

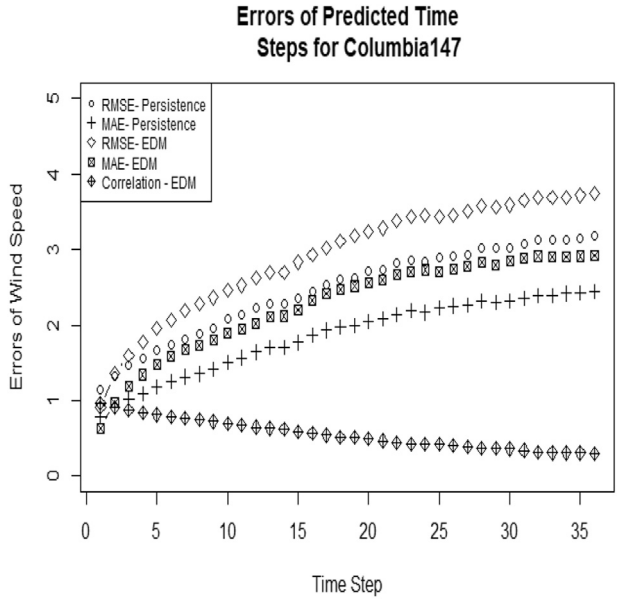

Fig. 19. Errors and correlations for Columbia147, RMSE (ms^{-1}), MAE (ms^{-1}) and correlations against time step for EDM and persistence.

respective height levels, occurred at most for the time steps of 2 and 9.

This model was also compared to the benchmark model of persistence. Wind speed persistence for a given site, as defined in [18],is a measure in which the duration of the average wind speed persists. The average for every multiple of the 6th hour was recorded as the value of persistence for the next consecutive 6 h or 36 time steps. This was done for the entire series of 2009 for all height levels for each station. The results are shown also in Figs. 17–21. It was determined that for Columbia and Blanchard at all height levels, our model out performed persistence for the first time step however for Neosho, persistence beat our model at all heights of the tall tower. This is expected as Nesoho, of the three stations, had the least annual mean friction velocity of 0.597 [11]. Our model, as expected, does better in more turbulent flow with greater roughness. It should be noted though, that the difference in the average RMSE for the EDM and the persistence model at all height levels of Columbia and Neosho did not exceed $0.5ms^{-1}$. This value was approximately $0.6ms^{-1}$ for Blanchard. This, thus demonstrates that the EDM is comparable to persistence. The model displays relatively good accuracy as for this short-term range, persistence, autoregressive, moving average, autoregressive moving average and autoregressive integrated moving average models all perform better than the NWP models [8]. However, the model displays better accuracy within the very short-term scale, between a few minutes to one hour. This is expected as persistence does well in the short term range. Another reason is due to the chaotic system's SDOIC [19]. The shorter term forecasts will be more accurate for these deterministic non-linear systems. The degree of accuracy was also determined by the amount of noise in the data. Since it is generally given that high wind speed implies high persistence [18], it would be expected that the model would not beat persistence for more time steps with increasing heights, and this is seen. We also got the expected result of the average difference between the two models for the 36 time steps to increase with increasing tower height. We obtained this result for two of three stations, Columbia and Blanchard. This small range in forecast where persistence can be beaten is also captured from the prediction horizon given by the LLE. From the results obtained, this is closest in agreement with the prediction horizon using the 90% confidence band and using a normalized error cap of 50%.

For this very short term forecast interval, there are not many research papers available [24]. However, another model used in a case study in Tasmania, Australia beat persistence in this scale, 2.5 min ahead. This is a hybrid model, Adaptive Neuro-Fuzzy Interface System (ANFIS) [24]. This very short term scale is utilized for efficient trading and optimal use of transmission lines [21]. There is no widespread acceptance in the industry for a particular very short-term forecasting system as there is no reliable forecasting technique for this scale where wind speeds have the most variations. Persistence is often deemed sufficient for this time scale as historically predicting for this scale was viewed as unnecessary [21].

4.5. Analysis of seasonality and the diurnal cycle

From Table 4, it is clear that for the slices and shifts of the data, all stations and height levels had a mean error of approximately 0 ms^{-1}. This is due to a roughly even distribution of negative and positive errors. They deviated from their respective means, for most cases, by an estimated value of 2 ms^{-1}. The exception was Blanchard137 after the first 6 h shift from $144m + 6$ slicing of the data, its deviation from the mean of approximately 0 ms^{-1} was an estimated wind speed value of 3 ms^{-1}.

The seasonality analysis was done for all three stations with particular concentration on Columbia as this station had all of the monthly data for 2009. In the Northern Hemisphere for the year of 2009, spring began on Friday 20th March. Summer started Saturday June 20th while for fall and winter they commenced on September 22nd and December 21st respectively. Spring corresponded to the 7272nd window. This coincided with a numeric value of forecast 3276. The start of summer 2009 corresponded with window 20520 which is numeric value 16524 whilst for fall and winter the windows values were 34056 and 47016 which coincided with numerical values of forecast 30060 and 43020 respectively.

Figs. 25–27 show the various errors for the four seasons in the forecast period in 2009 for Columbia68, Columbia98 and Columbia147 respectively. The seasons of spring, summer and fall will be of focus as winter of 2009 was represented as a few days in

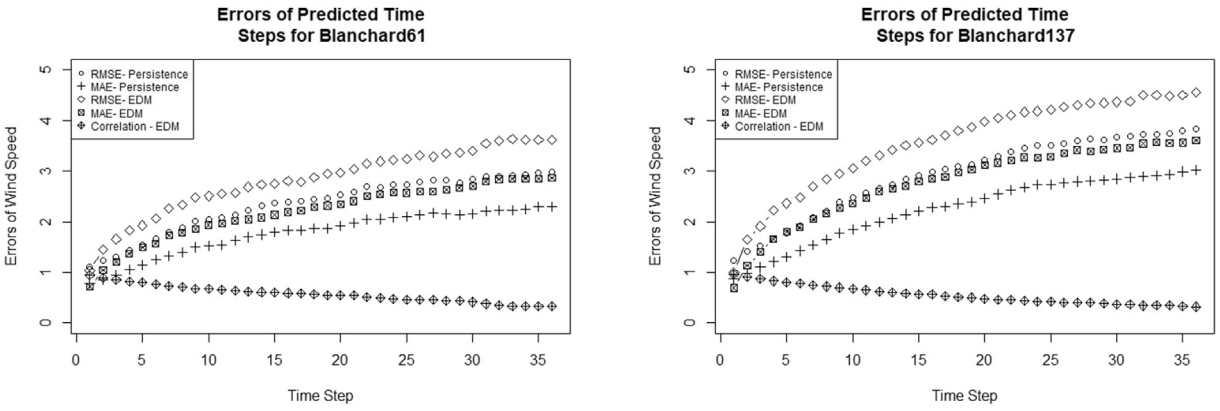

Fig. 20. Errors and correlations for Blanchard tall tower, RMSE (ms^{-1}), MAE (ms^{-1}) and correlations against time step for EDM and persistence.

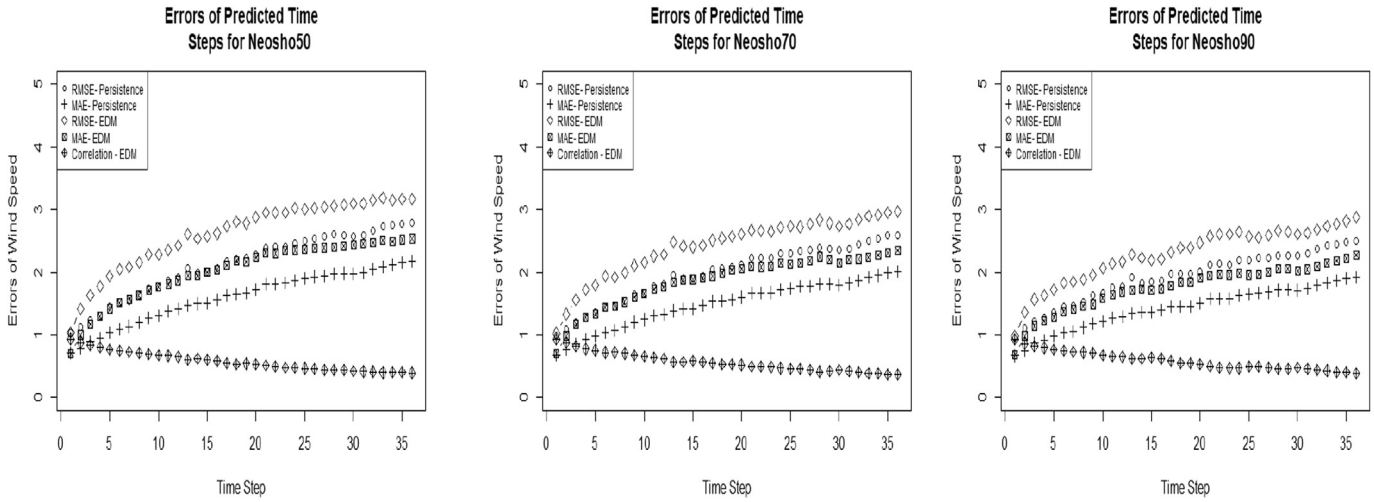

Fig. 21. Errors and correlations for Neosho tall tower, RMSE (ms^{-1}), MAE (ms^{-1}) and correlations against time step for EDM and persistence.

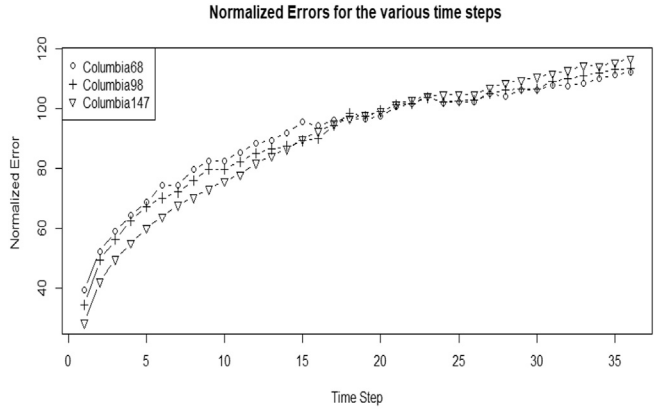

Fig. 22. Normalized Errors for height levels of Columbia Tall Tower, Normalized Errors (%) against Time Step.

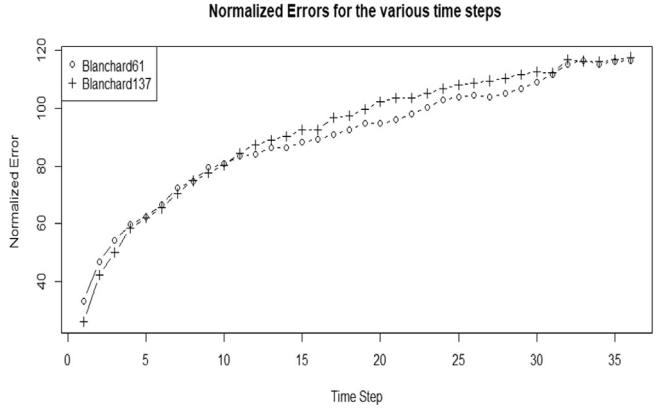

Fig. 23. Normalized Errors for height levels of Blanchard Tall Tower, Normalized Errors (%) against Time Step.

this analysis as data of 2010 were not included in this study. Also, since the data spanned one year, the seasonality aspect of the model could not be fully investigated. The average errors and standard deviations of these seasons were, however, determined and compared to that of the entire model run for 2009. It was given that for Columbia68, summer had the lowest magnitude of errors between model run and actual values; its value was −0.03809 with standard deviation of 1.511631. This is the only season whose average error was under the average error for the entire model run for 2009. Fall average errors were a bit higher than for the summer; their values were 0.064728 and 1.770366 respectively. Spring has the largest average errors and standard deviations; its values

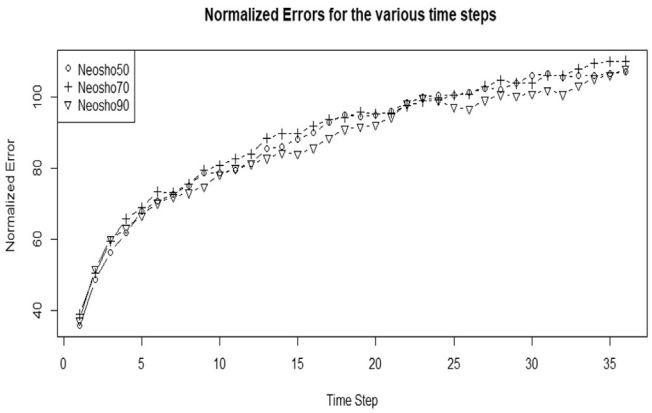

Fig. 24. Normalized Errors for height levels of Neosho Tall Tower, Normalized Errors (%) against Time Step.

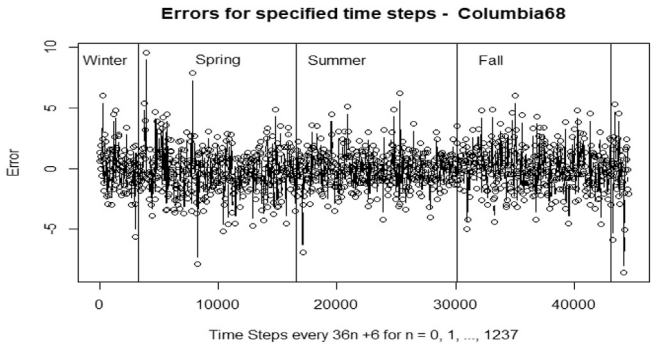

Fig. 25. Seasonality Analysis for Columbia68, Error (ms^{-1}) against Time Step every $36n + 6$.

were −0.19993 and 1.954639. This is expected as from the average wind speeds for the various months, shown in Ref. [1], summer had the least average wind speeds as well as incurred the least monthly variations. For Columbia98, once again summer had the least average errors in the simulation. The mean error was approximately the same as Columbia68 with the standard deviation increasing by an estimated 0.21. Fall, for this height level, had the highest error value of approximately 0.10 while spring had the lower value of 0.06. The standard deviation of the errors in the model, for spring were higher than for fall with an estimated value of 2.17 opposed to 1.82. Both summer and spring have lower average errors than the year model run, which from Table 4 is around 0.09. For the largest of the three height levels, Columbia147, all seasons considered were under the entire 2009 model run. Spring and summer both had the same average error of 0.05 while fall had a slightly smaller mean error value of 0.04. The standard

Table 4
Means, Standard Deviations, Min Values and Max Values of errors, in ms^{-1}, for various analyses.

Analyses	Station	Mean	Standard Deviation	Min Value	Max Value
36n+6	Columbia68	−0.04976043	1.791448	−8.6	9.6
	Columbia98	0.09388809	1.914046	−8.6	15
	Columbia147	0.08977431	2.064804	−9.4	10
144m + 6	Columbia68	−0.191192	1.679333	−5.05	6
	Columbia98	0.2311889	1.670056	−5.4	6.9
	Columbia147	0.1320323	2.066888	−8	6.7
36 + 144m + 6	Columbia68	0.07817742	1.819659	−5.9	9.6
	Columbia98	0.06601613	2.088458	−6.1	15
	Columbia147	−0.04369969	1.976215	−5.6	8.25
72 + 144m + 6	Columbia68	−0.1004072	1.800744	−7.9	5.3
	Columbia98	0.08013061	1.946351	−6.9	7.4
	Columbia147	0.1764266	2.11462	−9.4	10
108 + 144m + 6	Columbia68	0.01442377	1.857963	6.2	−8.6
	Columbia98	−0.002137463	1.929332	7.8	−8.6
	Columbia147	0.09463323	2.102374	9.7	−7.8
36n+6	Blanchard61	−0.1574112	2.063242	−6.6	10.9
	Blanchard137	−0.07311908	2.480952	−9.6	8.8
144m + 6	Blanchard61	−0.1845045	2.071191	−6.6	4.8
	Blanchard137	0.004801802	2.261244	−9.6	6.3
36 + 144m + 6	Blanchard61	−0.1805598	2.129216	−5.1	10.9
	Blanchard137	0.02518018	2.847701	−8.6	8.8
72 + 144m + 6	Blanchard61	−0.2122522	1.995355	−5	8.1
	Blanchard137	−0.5742613	2.379635	−9.05	7.1
108 + 144m + 6	Blanchard61	−0.05175725	2.068112	6.6	−6.6
	Blanchard137	0.2535688	2.335961	7.4	−6.05
36n+6	Neosho50	−0.007078053	2.050773	−9.8	12.5
	Neosho70	0.006690188	1.937222	−7.8	10.5
	Neosho90	−0.02743856	1.831548	−7.7	8.5
144m + 6	Neosho50	0.2418952	2.111877	−7.1	8.1
	Neosho70	0.01000672	2.003076	−7.8	7.7
	Neosho90	−0.1898185	1.839123	−7.1	5.6
36 + 144m + 6	Neosho50	−0.03209293	2.105925	−9.8	5.3
	Neosho70	0.1394792	1.853771	−7.2	8.8
	Neosho90	−0.07311972	1.724716	−7.7	5.25
72 + 144m + 6	Neosho50	−0.2335916	1.950025	−6.65	7.2
	Neosho70	−0.229328	1.865122	−6	6.9
	Neoaho90	−0.0705506	1.879079	−5.9	6.3
108 + 144m + 6	Neosho50	−0.004522849	2.015396	−6.7	12.5
	Neosho70	0.1066028	2.01141	−4.8	10.5
	Neosho90	0.2237346	1.864748	−5.23	8.5

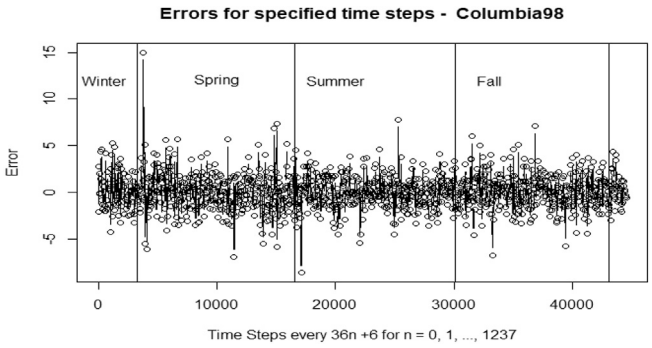

Fig. 26. Seasonality Analysis for Columbia98, Error (ms^{-1}) against Time Step every $36n + 6$.

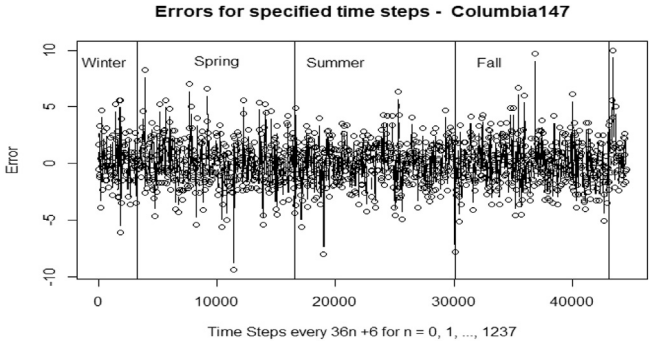

Fig. 27. Seasonality Analysis for Columbia147, Error (ms^{-1}) against Time Step every $36n + 6$.

deviation values were largest for spring (2.162856) and smallest for summer (1.896873). Thus, it was observed that for the station at Columbia, with the exception of the last height level in which all height levels incurred the same average deviations from the actual wind speed values, the summer season was the most accurate from this model. Also, for all heights on the tall tower, the standard deviations were largest for spring and smallest for summer.

For Blanchard61 and Blanchard137, all of the spring season was in the model run; however, for summer, 98 of the 376 readings of the slices representative of fall 2009 were missing. Similar statistics were calculated and it was observed that for the lowest height level there was larger average error and a lower standard deviation value for summer than spring, a magnitude difference of 0.2276 and 0.21228 respectively. For Blanchard137, summer had lower average errors and deviations when compared to spring. Considering station Nesoho at height level 50 m, once again, summer incurred the least average error of 0.017019 with standard deviation 1.936593 when compared to the other two seasons of spring and fall whose magnitude of average error were estimated 0.03 and 0.05 respectively. However, it must be noted that the fall season has 205 data slices missing from the 360 slices representative of fall 2009. For Neosho70, spring, however, had the least magnitude in its average error whose value is 0.00351 whilst the fall had the least standard deviation of 1.559813. For the final height level of Neosho, it was determined that the modulus of the average error for all the seasons considered were less than that value for the model run. This value as well as the standard deviation were the smallest for the summer season. Thus, four of the eight stations' height levels had the season of summer incurring the lowest magnitude of average errors and standard deviations. This is expected as the weakest winds occur during this season whilst the strongest winds are observed from October through spring. This is due to the passage of cyclones during these cooler periods. There is also during the summer, more heating which causes more instability and turbulence with less wind shear and near surface winds. The increased vegetation cover during this season are responsible as well for the increased turbulence due to its surface roughness and lower albedo and thus deeper boundary layer (BL) [11].

The diurnal analysis methodology, explained in Section 3.6, was investigated. The model took 56 days to initialize and it began to forecast on February 26th for all stations and height levels. The $144m + 6$ slicing of the forecast represents the extraction of the data every day at 6:50 a.m. The subsequent extracting of the data 6, 12 and 18 h later represented times of 12:50 p.m., 6:50 p.m. and 12:50 a.m. respectively. The results obtained for this slicing for the station of Columbia at height level 68 m are shown in Figs. 28–31. Statistical parameters for the entire forecast period for all slices and stations can also be viewed in Table 4.

Two cases occurred where the hours of 6:50 a.m. and 12:50 p.m. had the highest standard deviation values when compared to the early morning and evening hours of 12:50 a.m. and 6:50 p.m. This occurred for the lowest heights of Neosho and Blanchard. While for the highest levels of Columbia and Neosho we see the reverse occurrence where 6:50 p.m. had the highest standard deviation followed by 12:50 a.m., 6:50 a.m. and 12:50 p.m. This might be as a result of the nocturnal low level jet and strong overnight wind, which is common in the Midwest. This is due to the reduced convection and turbulence during the cool night hours which causes more stability with larger wind shear as a result of the reduced transfer of energy and momentum between the layers. The boundary layer is shallower and as such the geostrophic winds are closer to the surface [11]. However, there is no evident trend where a particular time of the day the model incurred more errors and greater standard deviations for all stations and heights. This may imply that the lack of sensitivity to the diurnal cycle by the stations height levels means that the model handles any transitions well.

5. Conclusions

Chaotic characteristics were established for wind speeds within Missouri for various height levels using both a qualitative method, phase space reconstruction, and a quantitative method, determination of the Lyapunov Exponent. Having established that the time series were chaotic in nature, a non-linear prediction algorithm was applied. Empirical Dynamical Modeling employed the dynamics of the time series instead of a set of governing equations. It was determined that this non-linear statistical method, which utilizes phase space reconstruction is relatively accurate as it is comparable to persistence. It however, beats this benchmark model for a prediction horizon of 1 time steps (10 min). It thus works best in the

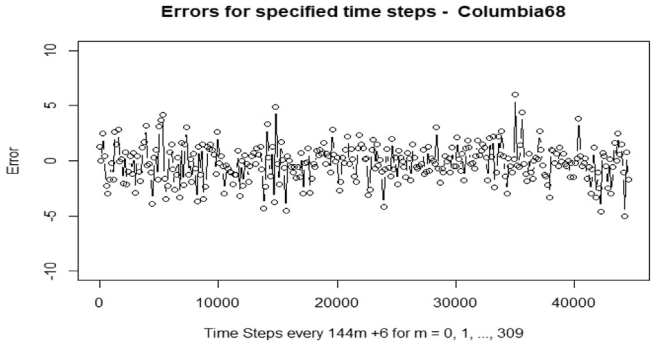

Fig. 28. Diurnal Analysis for Columbia68, Error (ms^{-1}) against Time Step every $(144m + 6)$.

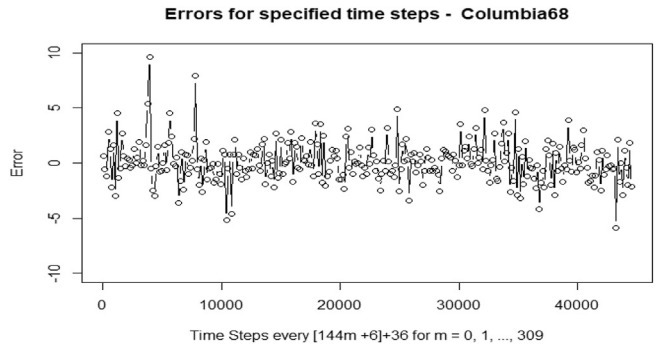

Fig. 29. Diurnal Analysis for Columbia68, Error (ms^{-1}) against Time Step every $[(144m + 6) + 36]$.

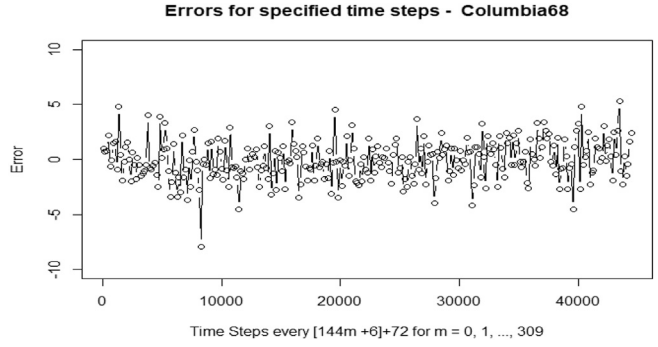

Fig. 30. Diurnal Analysis for Columbia68, Error (ms^{-1}) against Time Step every $[(144m + 6) + 72]$.

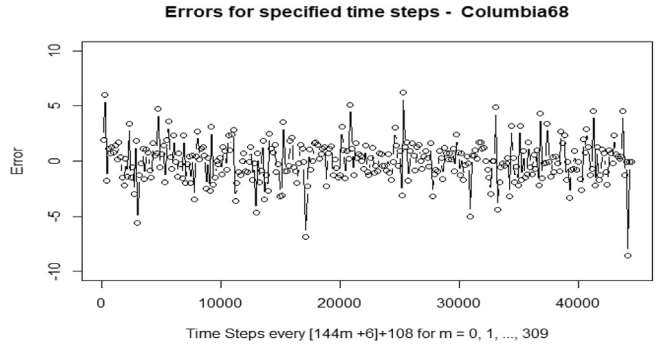

Fig. 31. Diurnal Analysis for Columbia68, Error (ms^{-1}) against Time Step every $[(144m + 6) + 108]$.

very short term as expected and predicted by prediction horizon given by the LLE. The normalized errors using a 50% cap also corroborate this time scale. This prediction model showed, as expected, the errors are increasing as the prediction time step increases; the errors eventually plateau. Seasonality and diurnal effects of the model were also investigated. It was shown that for the summer, four of the eight height levels had the lowest magnitude of average errors and standard deviations. This is expected, as there is less synoptic forcing in Missouri for the summer. It was also determined that the model handles the transitions of the diurnal cycle well as there is no time of day considered for which the model incurred more errors and had greater standard deviations for all stations and height levels.

The limitations of this study are due to the chaotic system suitability context that the data should be noise free and deterministic to fully capture the dynamics of multi-dimensional system by one observation. Thus forecasting using this method is not a simple task due to the non-linearity of the dynamical system and because the noise hides this dynamic [19].

It will be interesting to test this model with exogenous variables. Future work entails comparing the results obtained from this model with the findings from Artificial Intelligence (AI) methods such as Artificial Neural Network (ANN).

CRediT authorship contribution statement

Sarah Balkissoon: Conceptualization, Methodology, Software, Validation, Formal analysis, Investigation, Writing - original draft. **Neil Fox:** Conceptualization, Methodology, Validation, Formal analysis, Investigation, Data curation, Writing - review & editing, Supervision, Project administration. **Anthony Lupo:** Conceptualization, Methodology, Validation, Formal analysis, Investigation, Writing - review & editing, Supervision, Project administration. **Sue Ellen Haupt:** Conceptualization, Methodology, Validation, Formal analysis, Writing - review & editing. **Y. Charles Li:** Conceptualization, Methodology, Validation, Formal analysis. **Patrick Market:** Formal analysis, Investigation, Writing - review & editing. **Samuel Walsh:** Formal analysis, Investigation, Writing - review & editing.

Declaration of competing interest

The authors declare that they have no known competing financial interests or personal relationships that could have appeared to influence the work reported in this paper.

Acknowledgements

This study was made possible through the Fulbright Foreign Student Program. The authors would like to thank Dr. Samniqueka Halsey for aiding in the code automation process. We also extend our gratitude to the anonymous reviewers for all their suggestions. Funding for data collection was provided by Missouri Department of Natural Resources, Ameren UE, Aquila, Columbia Water and Light, Kansas City Power and Light, and Empire District Electric Company.

References

[1] S. Balkissoon, N. Fox, A. Lupo, Fractal Characteristics of Tall Tower Wind Speeds in Missouri, Renewable Energy, 2020.
[2] A. Brandstäter, J. Swift, H.L. Swinney, A. Wolf, J.D. Farmer, E. Jen, P. Crutchfield, Low-dimensional chaos in a hydrodynamic system, Phys. Rev. Lett. 51 (16) (1983) 1442.
[3] P. Bryant, R. Brown, H.D. Abarbanel, Lyapunov exponents from observed time series, Phys. Rev. Lett. 65 (13) (1990) 1523.
[4] M. Camplani, B. Cannas, The role of the embedding dimension and time delay in time series forecasting, Volumes, in: IFAC Proceedings 42, 2009, pp. 316–320, 7.
[5] L. Cao, Practical method for determining the minimum embedding dimension of a scalar time series, Phys. Nonlinear Phenom. 110 (1–2) (1997) 43–50.
[6] C.-W. Chang, M. Ushio, C.-h. Hsieh, Empirical dynamic modeling for beginners, Ecol. Res. 32 (6) (2017) 785–796.
[7] M. De Domenico, M.A. Ghorbani, Chaos and Scaling in Daily River Flow, 2010 arXiv preprint arXiv:*1002.0076*.
[8] N.C. De Freitas, M.P.d.S. Silva, M.S. Sakamoto, Wind speed forecasting: a review, Int. J. Eng. Res. Appl. 8 (4–9) (2018).
[9] J.-P. Eckmann, D. Ruelle, Fundamental limitations for estimating dimensions and Lyapunov exponents in dynamical systems, Phys. Nonlinear Phenom. 56 (2–3) (1992) 185–187.
[10] J.D. Farmer, J.J. Sidorowich, Predicting chaotic time series, Phys. Rev. Lett. 59 (8) (1987) 845.
[11] N.I. Fox, A tall tower study of Missouri winds, Renew. Energy 36 (1) (2011) 330–337.
[12] A.M. Fraser, H.L. Swinney, Independent coordinates for strange attractors from mutual information, Phys. Rev. A 33 (2) (1986) 1134.
[13] C. Garcia, G. Sawitzki nonlineartseries, Nonlinear Time Series Analysis 3, 2015.

R Package Version 0.2.
[14] H. Kantz, T. Schreiber, Nonlinear Time Series Analysis, vol. 7, Cambridge university press, 2004.
[15] S. Kawauchi, H. Sugihara, H. Sasaki, Development of very-short-term load forecasting based on chaos theory, Electr. Eng. Jpn. 148 (2) (2004) 55–63.
[16] M.B. Kennel, R. Brown, H.D. Abarbanel, Determining embedding dimension for phase-space reconstruction using a geometrical construction, Phys. Rev. A 45 (6) (1992) 3403.
[17] B. Kliková, A. Raidl, Reconstruction of phase space of dynamical systems using method of time delay, in: Proceedings of WDS 11, 2011, pp. 83–87.
[18] K. Koçak, A method for determination of wind speed persistence and its application, Energy 27 (10) (2002) 967–973.
[19] F. Lisi, V. Villi, Chaotic forecasting of discharge time series: a case study 1, JAWRA J. Am. Water Resour. Assoc. 37 (2) (2001) 271–279.
[20] N. Masseran, A.M. Razali, K. Ibrahim, W.W. Zin, Evaluating the wind speed persistence for several wind stations in Peninsular Malaysia, Energy 37 (1) (2012) 649–656.
[21] C.W. Potter, M. Negnevitsky, Very short-term wind forecasting for tasmanian power generation, IEEE Trans. Power Syst. 21 (2) (2006) 965–972.
[22] M.T. Rosenstein, J.J. Collins, C.J. De Luca, A practical method for calculating largest Lyapunov exponents from small data sets, Phys. Nonlinear Phenom. 65 (1–2) (1993) 117–134.
[23] K. Smith, G. Randall, D. Malcolm, N. Kelley, B. Smith, Evaluation of Wind Shear Patterns at Midwest Wind Energy Facilities, National Renewable Energy Lab., Golden, CO (US), 2002. Technical report.
[24] S.S. Soman, H. Zareipour, O. Malik, P. Mandal, A review of wind power and wind speed forecasting methods with different time horizons, in: North American Power Symposium, vols. 1–8, IEEE, 2010, 2010.
[25] J. Stark, Analysis of Time Series, Centre for Nonlinear Dynamics and its Applications, University Collage London, 1994.
[26] G.G. Szpiro, Forecasting chaotic time series with genetic algorithms, Phys. Rev. 55 (3) (1997) 2557.
[27] F. Takens, Detecting strange attractors in turbulence, in: Dynamical Systems and Turbulence, Warwick, Springer, 1980, pp. 366–381, 1981.
[28] K. Yu, Q. Yuan, C. Li, Y. Yang, Z. Xu, Comparative study of chaos identification methods for wind speed time series under different environmental measurement, Ekoloji Dergisi 107 (2019).
[29] M. Zeng, H. Jia, Q. Meng, T. Han, Z. Liu, Nonlinear analysis of the near-surface wind speed time series, in: 5th International Congress on Image and Signal Processing, IEEE, 2012, pp. 1893–1897, 2012.
[30] M. Zounemat-Kermani, O. Kisi, Time series analysis on marine wind-wave characteristics using chaos theory, Ocean Eng. 100 (2015) 46–53.